Geosciences Journal
Vol. 20, No. 5, p. 667 − 679, October 2016
DOI 10.1007/s12303-016-0005-1

Experimental and theoretical investigations into the formation of ice lenses in deformable porous media

Feng Ming*
Yu Zhang
Dong-qing Li

State Key Laboratory of Frozen Soil Engineering, Cold and Arid Regions Environmental and Engineering Research Institute, Chinese Academy of Sciences, Lanzhou 730000, China

ABSTRACT: The aim of this paper is to increase the understanding of ice lens initiation and growth in freezing soil. A model describing the growth process of ice lenses in soils has been established. The model presented here, which considers a series of processes, including heat transfer, water migration, phase change, ice lens formation, soil deformation, is solved by the use of a transient finite element. The simulated results agree with the experimental data. Results show that: (1) Negative pore water pressure occurs in unfrozen areas, this result in the water transfers from the unfrozen zone to the frozen zone and substantial water was stored in the frozen zone which results in oscillation with in water content distributions. (2) Few segregation ice lenses appeared in the fast freezing section, several thin and discontinuous segregation ice lenses appeared in the transitional section, and thick ice lenses appeared in the third phase when the freezing front tended to be stable. (3) Both the consolidation process and the expansion process are in progress during the freezing process, due to the migration of unfrozen water. (4) The frost heave model is composed of two aspects: the coupled heat-mass transport and the growth of ice lens. Numerical modeling is able to represent the development of both the thermal field and ice segregation observed in the physical models.

Key words: freezing soil, water-heat transfer, ice lens, tensile strength, mathematical model

1. INTRODUCTION

In cold regions, the ground is affected by significant periods of frost action. When fine-grained, moist soil is subjected to a freezing process, there is an observable expansion of volume. This phenomenon is known as frost heave. This phenomenon is partly responsible for beautiful surface patterns that appear in permafrost areas. However, the frost heave also causes damage to structures with footings placed in the frost susceptible soils above frozen depth. Previous studies indicate that frost heave can be attributed to ice lens formation associated with water migration to the freezing front and the development of segregation ice (Gilpin, 1980; O'Neill and Miller, 1985; Sheng et al., 1995; Bronfenbrener and Bronfenbrener, 2010). Therefore, it is important for us to understand how ice lenses grow in order to make accurate predictions of frost heave.

*Corresponding author: mf0329@163.com

Systematic studies of frost heave were performed early by Taber and in 1960s~1980s, further investigated of the studies were based on field and indoor tests. With the development of computer science, mathematical models of frost heave have been developed. Harlan (1973) presented two equations respectively describing the heat and water transfers in transient freezing process. His work has been further developed by Guymon and Luthin (1974) and Taylor and Luthin (1978). This theory has been referred to as the hydrodynamic model. The hydrodynamic model was considered to be too rough to modeling frost heave and could not deal with the formation of ice lenses (Rempel 2011).

The previous studies indicated that frost heave is a result of water migration and freezing (Harlan, 1973; Taylor and Luthin, 1978; Xu and Deng, 1991). However, many frost heave models have assumed that soil is incompressible, only consider heat and water transfer in the soil freezing process (Gilpin, 1980; O'Neill and Miller, 1985; Nixon, 1991; Cao and Liu, 2007). Thus, any consolidation that may occur due to pore water migration would not be taken into consideration. However, experimental results show that frost heave happens in the upper frozen zone while the consolidation occurs in the unfrozen zone (Mackay, 1974; Xu and Deng, 1991; Zhang et al., 2014). Several investigations illustrated that these changes in soil structure and void ratio were correlated with ice lens formation and growth (Michalowski and Zhu, 2006; Thomas et al., 2009). Furthermore, the void ratio and the soil structure change when soil is subjected to freeze-thaw cycles (Viklander, 1998). Consequently, a coupled flow and stress-strain analysis offers an improved insight into the system's behavior. Therefore, the deformation characteristics of soil should be taken into consideration with regard to ice lens growth in the frost heave model.

A large number of publications have investigated frost heave model that includes ice lenses formation (O'Neill and Miller, 1985; Sheng et al., 1995; Dash et al., 2006; Zhou and Zhou, 2012). These results indicate that frost heave is attributed to the formation of segregated ice lenses. Thus, frost heave models, which include the consideration of ice lenses,

required ice lens criteria. Based on an analysis and summary of the previous work, the conditions for the ice lenses formation can be divided into two types: (1) temperature criterion (Konrad and Morgenstern, 1980; Konrad and Duquennoi, 1993); (2) stress criterion (Takagi, 1979; Sheng et al., 1995; Thomas et al., 2009; Zhou and Zhou, 2012). The temperature criterion requires the segregation temperature. However, there is no specified method to determine the segregation temperature (Azmatch et al., 2012). Therefore, the stress criterion became the most common condition used after the concept of separation pressure was proposed by Takagi (1979). Gilpin (1980) presented the concept of disjoint pressure. However, due to the ambiguous concept of disjoint pressure, it is hard to determine the value of disjoint pressure (Nixon, 1991; Zhou and Zhou, 2012). The analysis above shows that stress criteria for initiating a new ice lens depend on pore ice (water) pressure, overburden pressure and separation strength. It can be seen that all the stress criteria discussed above generally ignore the influence of soil properties on ice lens formation. However, the experimental result shown that the cohesive force and tensile strength are directly influence the related to of the soil medium (He et al., 2000; Azmatch et al., 2011, 2012). Therefore, an understanding of the stress conditions that lead to ice lens initiation is necessary.

The key questions in reasonable frost heave models should be investigated, such as: firstly, unfrozen water content and water migration in soils. Porosity varies with the water and ice contents in the pore. In the previous models, Darcy law is generally adopted to simulate water migration (Giplin, 1980; Sheng et al., 1995; Thomas et al., 2009; Zhou and Zhou, 2012). Consequently, the driving force and hydraulic conductivity are important to determine the hydraulic field. Secondly, the formation and growth of ice lens (O'Nell and Miller, 1985; Sheng et al., 1995; Rempel, 2011). Well interpretation is helpful to determine the formation of ice lens and frost heave reasonably. It is well known that the soil freezing process involves coupled heat transfer, moisture transfer and force equilibrium, accompanied by pore water phase change. Thus, the driving force for water migration plays an important role in the freezing process.

Based on the previous literatures and our current laboratory tests, we present a mathematical model simulating ice lens growth in freezing soil. In this model, stress-strain equilibrium is incorporated along with heat and water transport. The hydraulic conductivity was adjusted to describe the unfrozen water gathering at the front of the ice lenses. The finite element algorithm is applied to solve the highly non-linear governing equations. Numerical simulations are completed with the assistance of COMSOL software. Finally, this model is in good agreement with experimental data on ice lens growth. It is further thought that this model may better explain the formation of ice lenses and may help to predict frost heave in freezing ground.

2. EXPERIMENTS

2.1. Experimental Conditions

Top-down freezing tests were conducted on soil columns in an open system. Figure 1 shows the schematic diagram of the experimental apparatus.

The tested material used for experiments is a silt clay taken from the Qinghai-Tibet Plateau which has a plastic limit of 14.4%, a liquid limit of 23.7%, a specific gravity of 2.72 g/cm^3. The sample was 100 mm in diameter and 100 mm in height, which has an initial water content of 16%, a dry density of 1.84 g/cm^3, and a freezing point of –0.15 °C. Figure 2 presents the grain-size distribution curve.

To start the test, the sample was placed in a constant temperature chamber and cooled to a uniform temperature of 3 °C. Then the desired pressure was applied to the top plate. Twenty-four hours later, the test began. The top plate temperature was changed to –2 °C, and the base plate temperature was maintained at 3 °C. The thermistors, 4 mm in diameter with an accuracy of 0.02 °C, were inserted into the soil sample at intervals of 1 cm. The sample container's side wall was

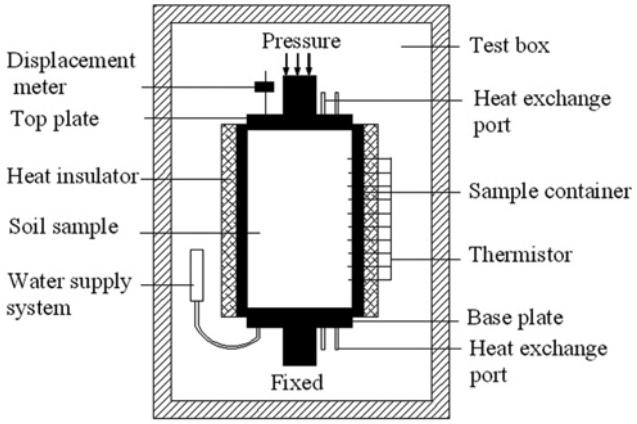

Fig. 1. Schematic diagram of the experimental apparatus.

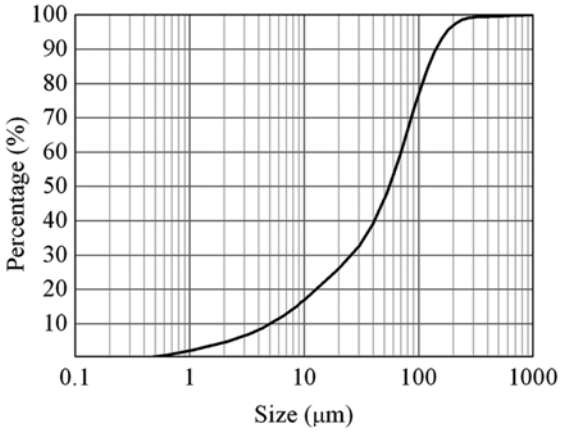

Fig. 2. Grain size distribution of soil sample.

Table 1. Experiment conditions

Test number	Controlling temperature (°C)		Overburden pressure (kPa)	Initial water content (%)	Temperature Gradient (°C/cm)
	Cold end	Warm end			
TN1	–2.0	3.0	0	16.02	0.50
TN2	–2.0	3.0	100	16.34	0.50
TN3	–2.0	3.0	200	16.17	0.50
TN4	–4.0	3.0	100	15.96	0.70
TN5	–6.0	3.0	100	16.09	0.90

heat-isolated and flow-isolated. A displacement meter (accuracy of 0.01 mm) was placed on the top end of the sample to measure the amount of frost heave. Water was applied freely at the base plate. The freezing time for each test was 72 h. Temperature and frost heave were recorded by the data collection system and saved in the computer. Finally, the sample was photographed and cut into layers 1 cm thick for water content determination. Five different experimental conditions are listed in Table 1.

2.2. Experimental Results

Figure 3 shows the temperature measured at five separate points in two samples. It can be seen that the temperature has different freezing rates in the different times. The temperature has a quick decrease in the fast freezing section (0–5 h) and a smaller decrease in the transition section (5–15 h). Finally, it tends to be in a stable thermal state in the stable section (15–72 h). Nearer to the cold end of the sample (9.5 cm), larger cooling amplitude is seen and less time (15 h) is required to reach the stable temperature (Fig. 3). Further from the top plate (1.5 cm), more time (30 h) is required for the temperature to decrease to a steady value.

During a freezing process, water will be constantly sucked into the soil due to the effect of cryogenic suction (Zhou et al., 2014). From Figure 4, it can be seen that there is an unsteady flow, i.e., the water intake flux changes as time passes. Even though, the curves can be divided into two portions: increase

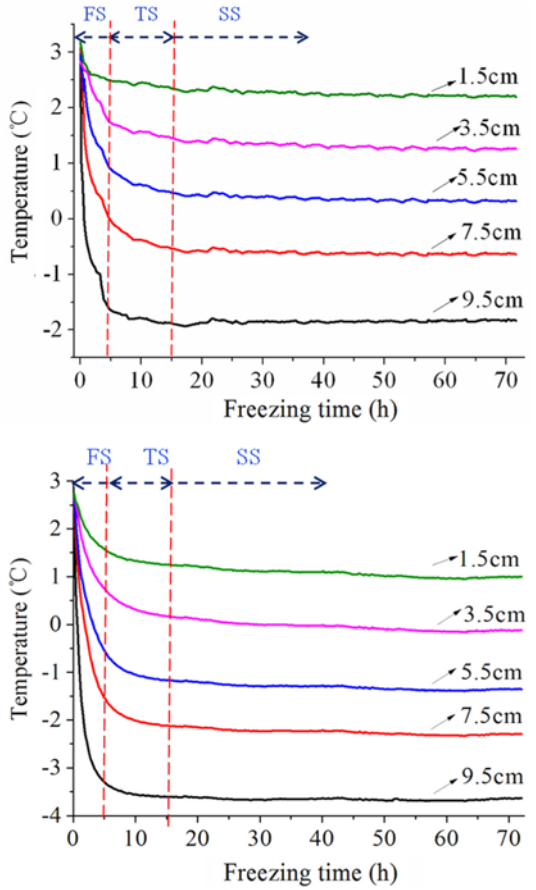

Fig. 3. Temperature change with time at different positions (FS: fast freezing section; TS: transition section; SS: stable section).

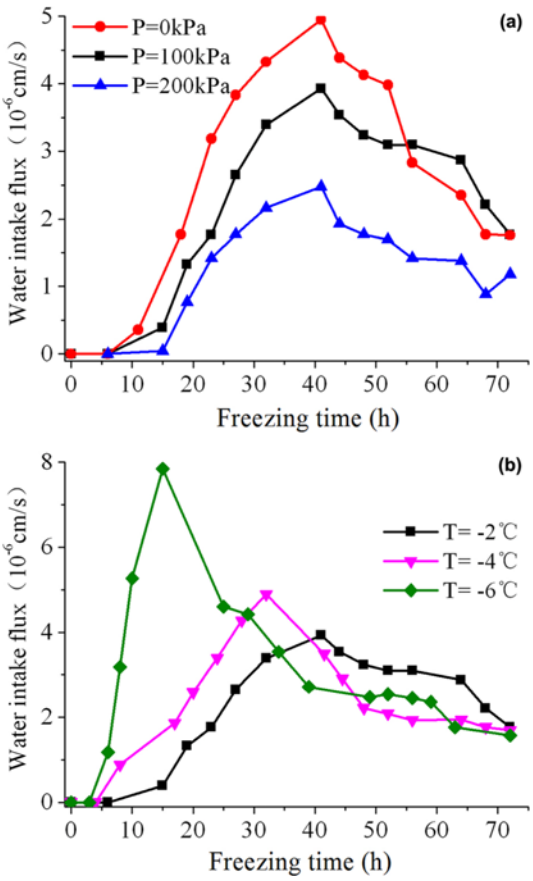

Fig. 4. Variations of water intake flux. (a) Different overburden pressures; (b) Different cold temperatures.

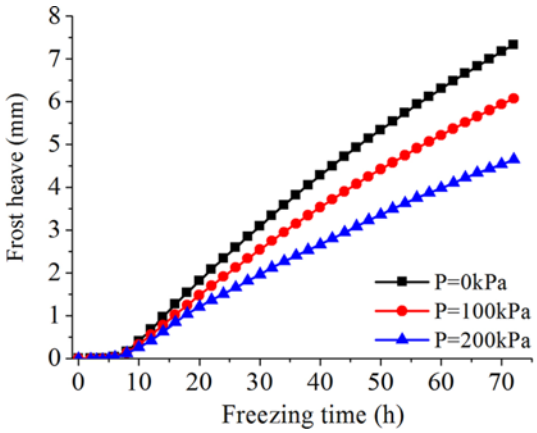

Fig. 5. Frost heave for typical one-sided freezing conditions.

phase and decrease phase. A change in overburden pressure from 0 kPa, 100 kPa to 200 kPa, resulted in a change in water intake flux from 4.89×10^{-6} cm/s, 3.82×10^{-6} cm/s to 2.63×10^{-6} cm/s, as shown in Figure 4a. The water intake flux decreased an increase of overburden pressure. A change in temperature from –2 to –4 °C, and then to –6 °C, resulted in a change in water intake flux from 3.82×10^{-6} cm/s, to 4.78×10^{-6} cm/s, and then to 7.84×10^{-6} cm/s. It can be seen that, under different temperature boundaries, the colder the top end temperature is, the less time the water intake flux will take to reach to the maximum, as shown in Figure 4b. Due to the unsteady water intake flux, the frost heave amount is different at different elapsed time. It can be seen that it is quite small in the fast freezing section, and then slightly increases (Fig. 5). Further, the overburden pressure at the level of 0, 100 kPa and 200 kPa, the frost heave is 7.33 mm, 6.07 mm, 4.65 mm, respectively (Fig. 5). It can be concluded that an increase in the overburden pressure results in a reduction in frost heave.

Many cracks exist in the frozen zone, but there are no cracks in the unfrozen zone (Fig. 6). It can be seen that ice strings are distributed horizontally and vertically to the direction of the heat flow. From top to bottom, the massive structure of ice strings appears in the range of 9–10 cm and then is followed by the layered structure of the ice lenses between 1–1.5 mm and 4 mm. This is because that when the heat flow is too rapid, however, insufficient water is drawn up to the freezing front (Rempel, 2011). Thus, there is no visible ice lens in the top end. When the frozen depth increases, the heat flow decreases, and sufficient water can be drawn to grow ice lenses. With unfrozen water supplied, the ice lenses thicken from top to bottom in the frozen zone. As a result, from top down, the thickness of the ice lenses increases from 0 to 4 mm (Fig. 6). It can be concluded that ice lenses formed different cryogenic structures in different sections due to the limited water supply.

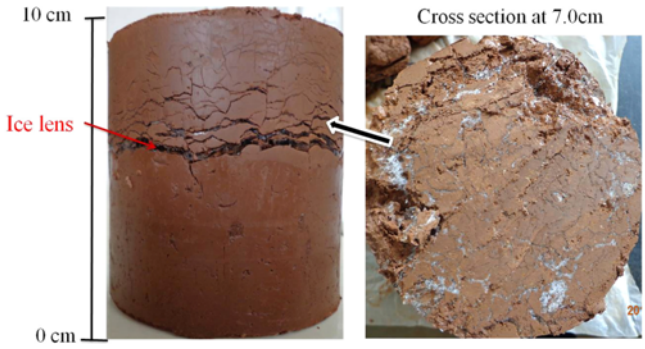

Fig. 6. Reticulate ice structure viewed in vertical sample section (TN2).

3. FROST HEAVE MODEL

Motivated by the experimental results, a frost heave model including mass and heat transport and ice lens segregation is presented in this section. The components of the model are presented in the following subsections. The process of water and heat coupling is assumed to be one-dimensional, with important assumptions as following:

(1) Soil is saturated, uniform, and isotropic.
(2) Water transfers in a liquid state through the soil.
(3) Soil grain and ice lenses are incompressible.
(4) The freezing point of water is assumed constant, ignored the depression under pressure.

3.1. Water Migration

The starting point for the research of ice lens growth is a basic physical understanding of the behavior of water migration in a thin layer near the surface of a solid substrate. Gilpin (1979, 1980) assumed that the water near the surface experiences a force of attraction acting toward the solid and developed a model of water migration in such a condition.

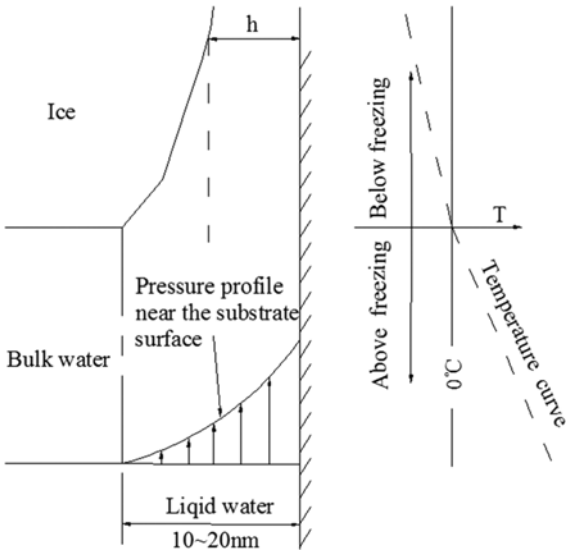

Fig. 7. Liquid layer near a substrate (h is the thickness of the liquid layer).

In this paper, we only introduce some necessary results and the details about Gilpin's theory can be found in his paper (Gilpin 1979; 1980). Figure 7 schematically illustrates the liquid layer near a solid substrate extending from a region above the freezing point into a region below freezing.

According to the definition of Gibson free energy, the free energy of the water G_L with a distance y from the solid substrate surface can be describe as

$$G_L = G_{L0} + V_L P_{Ly} - S_L T_L - g(y). \quad (1)$$

The free energy of the ice G_S at some point along the interface is

$$G_S = G_{S0} + V_s P_S - S_S T_S, \quad (2)$$

where G_{L0} and G_{S0} is the Gibson free energy of water and ice at the reference state, respectively; V_L and V_S are specific volumes of the liquid and the solid phases, $V_L = 1/\rho_w$, $V_S = 1/\rho_i$; P_{Ly} and P_S are pressure in liquid and solid phases; S_L and S_S are entropy of liquid and solid; T_L and T_S are temperature in liquid and solid phases; $g(y)$ is the effect from the surface of the solid substrate.

Equating the liquid and solid free energies at the interface results in the following expression,

$$G_{L0} + V_L P_{Ly} - S_L T_L - g(y) = G_{S0} + V_s P_S - S_S T_S. \quad (3)$$

The reference conditions can be chosen such that $G_{L0} = G_{S0}$. Also, the temperature cannot change discontinuously across the phase boundary, so that $T_L = T_S = T$. Then Equation (3) can be rewritten as,

$$g(y) = V_L P_{Ly} - V_s P_S - T(S_L - S_S). \quad (4)$$

Also, the liquid pressure P_{Lh} at $y = h$ can be written as

$$P_{Lh} = g(h)/V_L + V_s P_S/V_L + TL/T_a V_L, \quad (5)$$

where h is the local thickness of the unfrozen layer; $L = T_a(S_L - S_S)$; $T_a = 273.15$ K.

Choosing 1 atm as the reference pressure, the equivalent water pressure P_w can be defined as

$$P_w = P_{Lh} - g(h)/V_L, \quad (6)$$

where P_w is the equivalent water pressure.

After treating the interface as a plane and assuming the upward movement of the ice lens is a quasi-static process, the boundary condition of P_w at the warm end of the ice lens is obtained by substitution Equation (5) into Equation (6) and some transformations

$$P_w = \frac{V_s}{V_L} P_{ob} + \frac{LT}{V_L T_0}, \quad (7)$$

where P_{ob} is the overburden pressure.

3.2. Mass Conservation Equations

The law of mass conservation of the moisture for freezing soil can be expressed as

$$\frac{\partial}{\partial t}(m_i + m_w) = -\rho_w \frac{\partial v_w}{\partial z}, \quad (8)$$

where m_i is the mass of ice; m_w is the mass of water; z is positive upwards; ρ_w is the density of liquid water and v_w denote volumetric liquid.

The mass of ice and water in a unit volume can be written as

$$m_i = n\theta_i \rho_i, \; m_w = n(1-\theta_i)\rho_w, \quad (9)$$

where n is the porosity of soil. θ_i is the ice volume saturate; ρ_i is the density of ice.

In order to reduce the number of unknowns in Equation (8), we bring to bear some additional relations. We assume that when a frozen fringe is present the flow toward the ice lens is adequately described by Darcy's law:

$$v_w = -k \frac{\partial P_w}{\partial z}, \quad (10)$$

where k is hydraulic conductivity.

Substituting Equation (10) into Equation (8) gives

$$\frac{\partial}{\partial t}[\rho_i n \theta_i + \rho_w n(1-\theta_i)] = \rho_w \frac{\partial}{\partial z}\left(k \frac{\partial P_w}{\partial z}\right). \quad (11)$$

Rearranging Equation (11) gives

$$\frac{\rho_i \theta_i + \rho_w (1-\theta_i)}{\rho_w} \frac{\partial n}{\partial t} + \frac{n(\rho_i - \rho_w)}{\rho_w} \frac{\partial \theta_i}{\partial T} \frac{\partial T}{\partial t} = k \frac{\partial}{\partial z}\left(\frac{\partial P_w}{\partial z}\right). \quad (12)$$

3.3. Energy Conservation Equations

As the freezing process requires a temperature gradient in the soil, the frost heave model should include a heat transfer law. The ice content in the unit volume of soil is $n\theta_i$, so in unit time, the latent heat generated by the increment of ice content is $L_{\rho i} \frac{\partial n\theta_i}{\partial t}$, and the heat taken away by water flow is $C_w v \frac{\partial T}{\partial x}$. According to the law of conservation of energy, the equation of thermal diffusion (one-dimensional) can be described as (Michalowski and Zhu, 2006).

$$\frac{\partial}{\partial z}\left(\lambda \frac{\partial T}{\partial z}\right) - C_w v_w \frac{\partial T}{\partial z} = C \frac{\partial T}{\partial z} - L\rho_i \frac{\partial n\theta_i}{\partial t}. \quad (13)$$

Rearranging Equation (13) gives:

$$\left(C - Ln\rho_i \frac{\partial \theta_i}{\partial T}\right) \frac{\partial T}{\partial t} - L\rho_i \theta_i \frac{\partial n}{\partial t} = \frac{\partial}{\partial z}\left(\lambda \frac{\partial T}{\partial z}\right) - C_w v_w \frac{\partial T}{\partial z}. \quad (14)$$

The volumetric heat capacities C and the coefficients of heat conductivity λ, including soil grain, water and ice are calculated by the following formulas (Nicolsky et al., 2009).

$$C = (1-n)C_s + n(\theta_i)C_w + n\theta_i C_i, \quad (15)$$

$$\lambda = \lambda_s^{1-n}\lambda_i^{n\theta_i}\lambda_w^{n(1-\theta_i)}, \quad (16)$$

where C_s, C_w and C_i are the volumetric heat capacities of soil grain, water and ice, respectively; λ_s, λ_i and λ_w are the coefficients of heat conductivity of soil grain, ice and water, respectively.

3.4. Deformation of Freezing Soil

The behavior of frozen soils commonly assumed as that of an elastic solid (Thomas et al., 2009; Zhou and Li, 2012). In reality, the total strain is taken as a sum of the elastic strain increment, the creep strain increment and the thermal strain increment. The strain can be written as

$$\varepsilon = \varepsilon^e + \varepsilon^T + \varepsilon^c, \quad (17)$$

where ε is the total strain increment, ε^e is the elastic strain increment, ε^T is the increment caused by temperature and ε^C is the creep strain increment.

The thermal strain can be described as

$$\varepsilon^T = R(T - T_i), \quad (18)$$

where R is the coefficient of thermal expansion, and $R = 2 \times 10^{-6}$; T_i is the initial temperature.

The creep equation of frozen soil is defined by the compression and tension test under the uniaxial state of stress (Xu et al., 1991). The regression parameters in Equation (19) are shown in Table 2.

$$\varepsilon^c = \frac{A\sigma_p^B t^C}{(1+|T|)^D}, \quad (19)$$

where, A, B, C, and D are regression parameters; t is the time; σ_p is the applied pressure.

The compression curve of soil gives,

$$d\sigma' = -dE_s\varepsilon^e, \quad (20)$$

where σ' is effective stress; ε^e is elastic strain increment; E_s is modulus of compression, which can be determined from the laboratory test, and was assumed as a constant in the numerical simulation.

Substituting Equations (18)–(20) into Equation (17) gives:

$$d\sigma' = -dE_s\left[\varepsilon - R(T - T_i) - \frac{A\sigma_p^B t^C}{(1-T)^D}\right]. \quad (21)$$

The relationship between strain and porosity can be described as

$$\varepsilon = \frac{n_0 - n}{1 - n}, \quad (22)$$

where n is porosity; n_0 is the initial porosity.

The relationship between deformation Δh and porosity n is:

$$\Delta h = \int_0^{z_0} \frac{n_0 - n}{1 - n} z_0. \quad (23)$$

3.5. Criterion of Ice Lens Formation

In the introduction, the conditions for ice lens formation have been discussed. Based on an analysis and summary of the previous work, the stress criterion approach has been adopted. From the analysis of freezing process, we cleared the stress criterion of ice lens formation. It can be seen that the soil particles were connected by the unfrozen water film (Fig. 8a). Thus, the relative pressure of the liquid layer at the ice-water interface P_{Lh} is, the contact stress between soil particles, which is also called the disjoining pressure (Derjaguin and Churaev, 1978). With the temperature decreasing, the thickness of unfrozen water film decreasing (Fig. 8b). Due to the phase interface closer to the solid surface, the relative pressure of the liquid layer at the ice-water interface P_{Lh} (disjoining pressure) gradually increasing. After the contact of soil particles were destroyed, the ice lens formed (Fig. 8c). The question is then 'At what pressure will the force the pressure at the contact point drop to zero, allowing the ice to separate the soil particles?'

The experimental results show that pore ice pushes the structure of the soil grain against its tensile strength and overburden pressure, causing it to fracture via unfrozen film water (Akagawa et al., 2006; Azmatch et al., 2011). Azmatch et al. (2012) pointed out that the stress state and tensile strength of soil govern ice lens growth because they control the number of vertical cracks and vertical ice lenses. Thus, based on the stress criterion for initiating a new ice lens (Gilpin, 1980), the sum of overburden pressure P_{ob} and tensile strength σ_t

Table 2. Physical parameters for modeling freezing soils

Parameter	value	Parameter	value	Parameter	value
α	–5	ρ_s (kg/m^3)	2710	λ_s (W/(m·°C))	1.20
β	–8	ρ_i (kg/m^3)	917	λ_i (W/(m·°C))	2.22
A	0.55	ρ_w (kg/m^3)	1000	λ_w (W/(m·°C))	0.58
B	2.1	P_a (Pa)	1.01×10^5	C_s (J/(kg·°C))	800
C	–0.15	g (m/s^2)	9.81	C_i (J/(kg·°C))	2044
D	4.5	k_0 (m/s)	2.15×10^{-8}	C_w (J/(kg·°C))	4180
E_s (MPa)	12	σ_t (kPa)	110	L (J/kg)	3.34×10^5

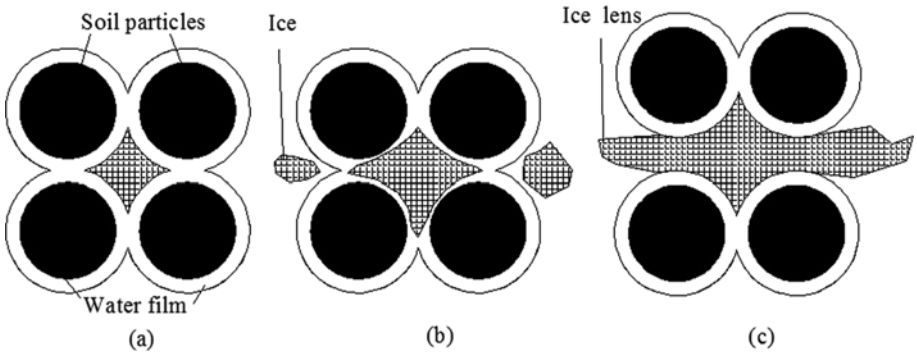

Fig. 8. Schematic diagram of ice lens formation.

is adopted as the separation strength. As a consequent, the criterion of ice lens formation equation can be written as:

$$P_{Lh} \geq P_{ob} + \sigma_t . \tag{24}$$

The pressures can be different, if the interface is curved. The difference is (Gilpin, 1980).

$$P_s - P_{Lh} = \sigma_{SL}\overline{K} , \tag{25}$$

where σ_{SL} is the ice-water interfacial tension; $\overline{K}$ is the mean curvature of the interface.

Substituting Equation (25) into Equation (5) gives,

$$g(h) = P_{Lh}(V_L - V_s) - \sigma_{SL}\overline{K}V_s - TL/T_0 . \tag{26}$$

Substituting Equation (26) into Equation (6) gives,

$$P_{Lh} = (V_L P_w - V_s\sigma_{SL}\overline{K} - TL/T_0)/V_s . \tag{27}$$

Notably, when a new ice lens starts to form, the effective stress vanishes and the disjoining pressure bears the total overburden pressure. Thus, the disjoining pressure P_{Lh} can be expressed as:

$$P_{Lh} = \begin{cases} (V_L P_w - V_s\sigma_{SL}\overline{K} - TL/T_0)/V_s & P_{Lh} < P_{ob} + \sigma_t \\ P_{ob} & P_{Lh} \geq P_{ob} + \sigma_t \end{cases} . \tag{28}$$

4. NUMERICAL SIMULATION

4.1. Method of Dispersing Equations

Equations (12) and (14) are highly nonlinear because the coefficients in these equations vary with time and they will affect each other. Thus, they were solved with the assistance of COMSOL software. The governing Equations (12) and (14) could be given in the following general form

$$Q_a\frac{\partial\chi}{\partial t} + \nabla\cdot\Gamma = q , \tag{29}$$

where χ is the variable in the governing equations, $\chi = \{T, n\}$. Q_a is the damping coefficient. Γ is flux vector and q is the source term.

Generalized solution to Equation (29) can be written as following,

$$\left(Q_a\frac{\partial\chi}{\partial t}, \overline{\chi}\right)_\Omega + (\nabla\cdot\Gamma, \overline{\chi})_\Omega = (q, \overline{\chi})_\Omega\Omega , \tag{30}$$

where $\overline{\chi}$ is virtual displacement. Equation (30) could be written as,

$$\left(Q_a\frac{\partial\chi}{\partial t}, \overline{\chi}\right)_\Omega - (\Gamma\cdot\nabla\overline{\chi})_\Omega = (q, \overline{\chi})_\Omega + (n\cdot\Gamma, \overline{\chi})_{\partial\Omega} . \tag{31}$$

The time terms are discretized by using backward difference

$$\frac{\partial\chi}{\partial t} = \frac{\chi^i - \chi^{i-1}}{\Delta t} , \tag{32}$$

where the superscript i refers time i, i–1 for time i–1. Ω is calculating domain. $\partial\Omega$ is the boundary of the calculating domain, and n is the outward normal unit vector of boundary. Substituting Equation (32) into Equation (31) and gives,

$$\left(Q_a\frac{\chi^i - \chi^{i-1}}{\Delta t}, \overline{\chi}\right)_\Omega - (\Gamma\cdot\nabla\overline{\chi})_\Omega = (q, \overline{\chi})_\Omega + (n\cdot\Gamma, \overline{\chi})_{\partial\Omega} . \tag{33}$$

Rewriting Equation (33) and gives,

$$(Q_a\chi^j, \overline{\chi})_\Omega - \Delta t(\Gamma, \nabla\overline{\chi})_\Omega = \Delta t(q, \overline{\chi})_\Omega + \Delta t(n\cdot\Gamma, \overline{\chi})_{\partial\Omega} + (Q_a\chi^{j-1}, \overline{\chi})_\Omega . \tag{34}$$

Stable scheme is employed for variable χ, that is

$$\chi = \frac{\chi^i + \chi^{i-1}}{2} . \tag{35}$$

Finally, Equation (35) could be rewritten as

$$2(Q_a\chi^j, \overline{\chi})_\Omega - \Delta t(\Gamma, \nabla\overline{\chi})_\Omega = 2\Delta t(q, \overline{\chi})_\Omega + 2\Delta t(n\cdot\Gamma, \overline{\chi})_{\partial\Omega} + 2(Q_a\chi^{j-1}, \overline{\chi})_\Omega - \Delta t(Q_a\chi^{j-1}, \overline{\chi})_\Omega . \tag{36}$$

The following form is defined in the above equation,

$$(q_1, q_2)_\Omega = \int_\Omega (q_1, q_2)d\Omega , \tag{37}$$

where q_1 and q_2 are two factors of each term in equation, such as $q_1 = Q_a \chi^i$ and $q_2 = \overline{\chi}$ in the first term at the left of Equation (36).

4.2. Initial and Boundary Conditions

The initial condition can be given by

$$\chi(x, y, z, 0) = \chi_0, \tag{38}$$

where χ_0 is a known function of time or a prescribed value of variable χ at the initial time.

There are two types of boundary conditions included in the above model.

(1) The first type of condition is Dirichlet boundary condition

$$\chi|_{bc} = \overline{\chi}_{bc}, \tag{39}$$

where $\overline{\chi}_{bc}$ is the prescribed value of variable χ at the boundary $\chi|_{bc}$.

(2) The second type of condition is Neumann boundary condition:

$$n \cdot \Gamma = R + (\partial \Pi / \partial \chi)_{\mu}^{T}, \tag{40}$$

where n is the outward normal unit vector of boundary, R is source term at boundary, $(\partial \Pi / \partial \chi)_{\mu}^{T}$ is a matrix designated for the flexibility of the constraint type, and μ is the matrix of Lagrange multiplier.

4.3. Auxiliary Parameters

θ_i is the ice volume saturate, which can be expressed as (Thomas et al., 2009).

$$\theta_i = \begin{cases} 1 - [1 - (T - T_0)]^{\alpha} & T \le T_0 \\ 0 & T > T_0 \end{cases}, \tag{41}$$

where α is the experimental coefficient, which can be determined by the measured relation between the volumetric unfrozen water content and temperature: T is the soil temperature, and T_0 is freezing point of pore water (both in Celsius temperature).

According to previous studies (Thomas et al., 2009; Zhou and Li, 2012), the new ice will block the water flow to the old ice lens. Thus, the hydraulic conductivity k can be written as

$$k = k_0 [1 - (T - T_0)]^{\beta}, \tag{42}$$

where k_0 is the hydraulic conductivity when the soil is fully unfrozen, and β is a soil parameter, $\beta = -8$ is adopted to represent a typical soil such as a Calgary silty clay (Patterson and Smith, 1981).

The soil thermo-physical properties of the soil were measured in the laboratory. Creep parameters (A, B, C, and D) of frozen soil were determined by tests. The parameters are listed in Table 2.

5. SIMULATION RESULTS

The predicted ice lens distribution at different times is shown in Figure 9, the black and white sections denote the soil and ice lenses respectively. At the top of the sample, due to a high temperature gradient close to the cold end, there is not sufficient time for water transfer. Thus, the ice lenses in the top are invisible, although they had initialized. With the rate of the freezing front penetration decreases, larger ice lenses at a greater spacing form progressively in the column. Due to the supply of unfrozen water, the ice lenses become thicken from top to bottom in the frozen zone. Furthermore, many multilayered ice lenses exist in the numerical results. Such predicted ice lens distributions are consistent with experimental observations in freezing tests (Zhou and Zhou, 2012).

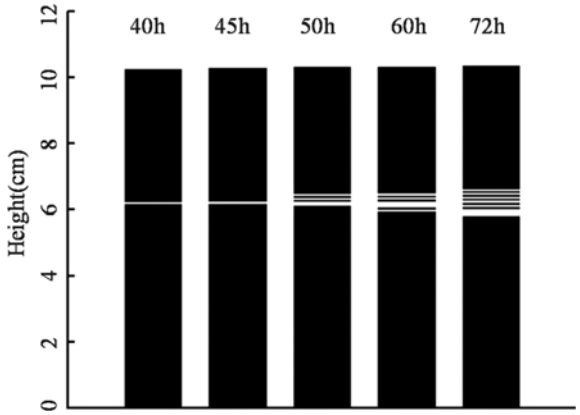

Fig. 9. Predicted ice lens distributions (white: ice lens).

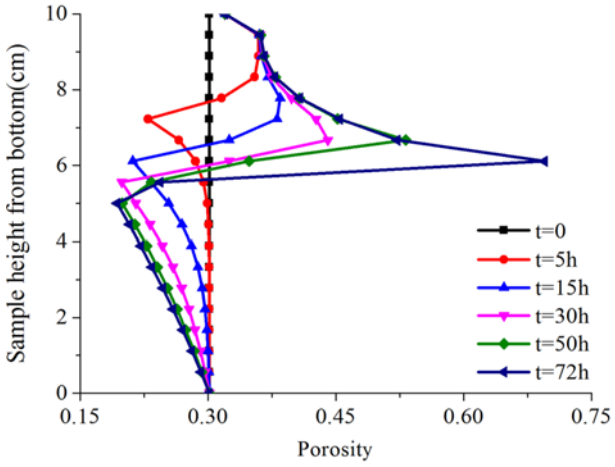

Fig. 10. Distribution of porosity at different times (the top plate temperature was –2 °C, P_{ob} = 100 kPa).

The changes in porosity at different times are shown in Figure 10. It can be seen that at any time, the porosity increased in the frozen zone and decreased in the unfrozen zone. As is shown in Figure 10, the further the distance is between a given point and the freezing front, the less the porosity at that point will decrease. For example, at the early time of t = 5 h, in the range of 6~7.5 cm, the porosity is smaller than the initial value. Due to water migration from the unfrozen zone to the frozen zone, the porosity increased. According to Equation (23), the change of the porosity reflects the soil deformation. However, there is some difference. The deformation in the unfrozen zone is caused by consolidated, while the deformation in the frozen zone is caused by frost heave (Fig. 10). As a consequence, the frost heave measured was the sum of deformation in the unfrozen zone plus the deformation in the frozen zone.

The water in the liquid film plays an important role in the growth of the ice lens, as seen in Figure 11, in the region of the frozen fringe the development of a gradient of pore water pressure results both in an opposing development of a pore pressure gradient that, to some degree, counteracts the upward water flow drawn by the negative pore pressure. Figure 11 shows the pore water pressure profiles at different positions. According to Equation (28), when the disjoint pressure P_{Ly} reaches $P_{ob} + \sigma_t$, a new ice lens is initiated in the frozen fringe. After a new ice lens is formed, the local disjoint pressure falls to the overburden pressure, as has also been observed by Konrad and Morgenstern (1980) and Nixon (1991). According to Figure 7, the warmest ice lens is connected to the pore water directly, so the disjoining pressure is also the pore-water pressure in the unfrozen zone. A negative pore water pressure appears in the unfrozen zone under the frozen fringe. Due to water migration, the consolidation process and the expansion process occur in the freezing process.

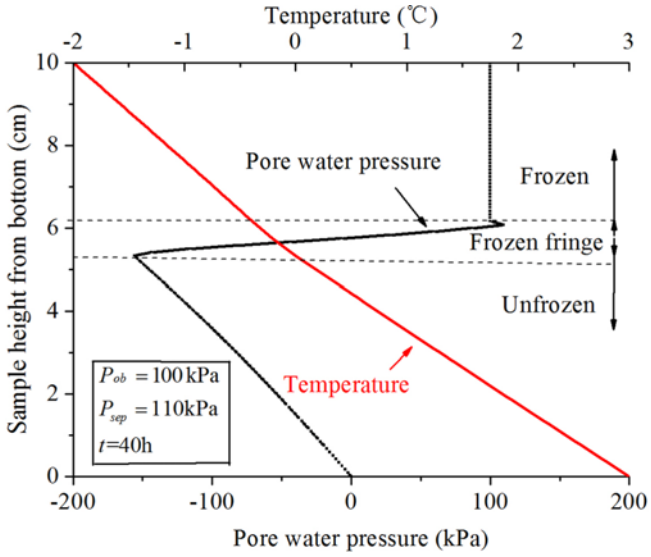

Fig. 11. Pore water pressure distributions along with height of specimen (the top plate temperature was –2 °C, P_{ob} = 100 kPa).

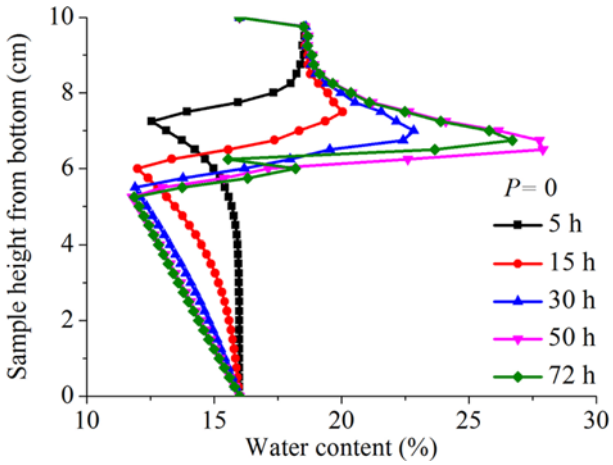

Fig. 12. Water content distributions (the top plate temperature was –2 °C, P_{ob} = 100 kPa).

Owing to the different negative pore water pressure, different degrees of consolidation occurred in the unfrozen soil. As a consequence, the rate of porosity decrease in the unfrozen soil is different, as shown in Figure 10.

Water content w is the mass ratio of the sum of pore water and pore ice to the soil grains, and can be described as $w = \frac{\rho_i n\theta_i + \rho_w n(1-\theta_i)}{(1-n)\rho_s}$. From Figure 12, it can be seen that water content is distributed through oscillation along the column. When a temperature gradient is formed between the frozen and unfrozen zones, a suction gradient develops in the frozen zone in response to any temperature gradient and water migrates from the unfrozen zone through the continuous unfrozen water films into the frozen zone. Due to the large rate of freezing front penetration, less water migrated at 8~10 cm (Fig. 12). As the freezing front moves down slowly, the water has enough time to 6~8 cm. It can be seen that in the range of 6–8 cm, there were many ice lenses (Fig. 9). This indicates that a lot of water was stored in the frozen zone in the form of ice lenses. Therefore, it is not difficult to explain that, due to the penetration of the freezing front, the location of maximum water content is further down.

6. COMPARISION WITH EXPERIMENTAL RESULTS

The comparison between tested results and simulation results is presented in this section.

When a temperature below freezing point was applied to the top of the soil column, the freezing front moved down gradually (Fig. 13). The freezing front descends quickly at the beginning and then descends slowly at a steady rate. Finally, the frozen depth shows little change. This change trend is similar to the experimental results presented by Konrad and Morgenstern (1981). Above the freezing front curve is the frozen zone and the unfrozen zone lies underneath. Under overburden pressures of 0 and 100 kPa, the position of the freezing fronts tested lies on 5.28 and 5.22 cm, while the

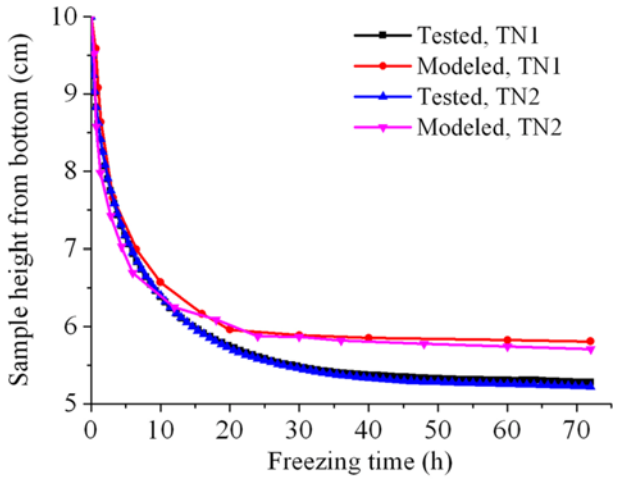

Fig. 13. Freezing front position in test TN1 and TN2.

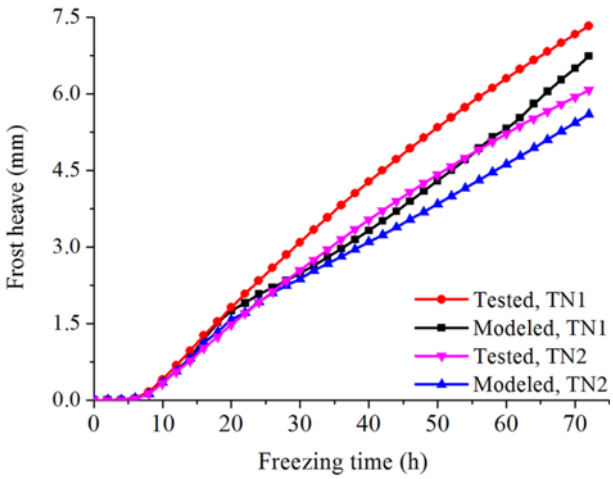

Fig. 15. Frost heave in tests TN1 and TN2.

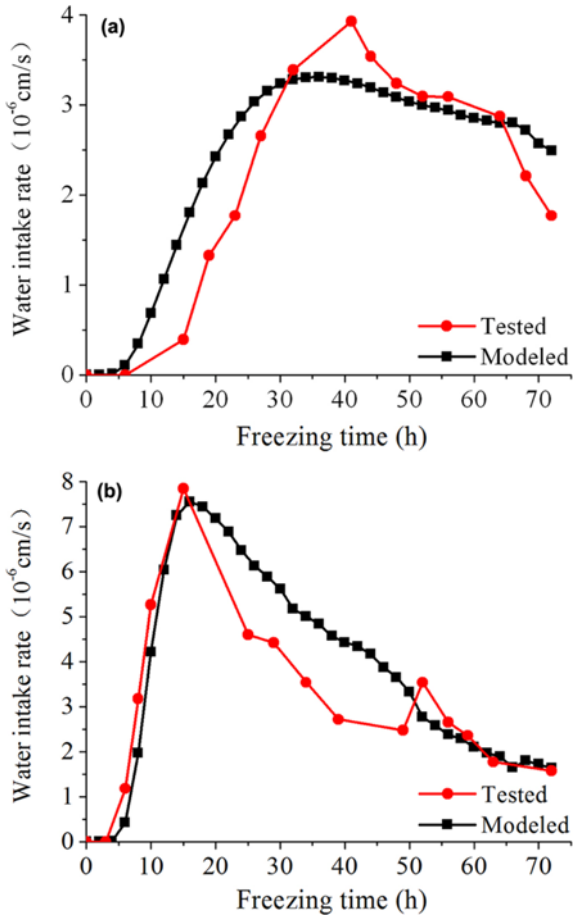

Fig. 14. Water intake flux. (a) In test TN2; (b) In test TN5.

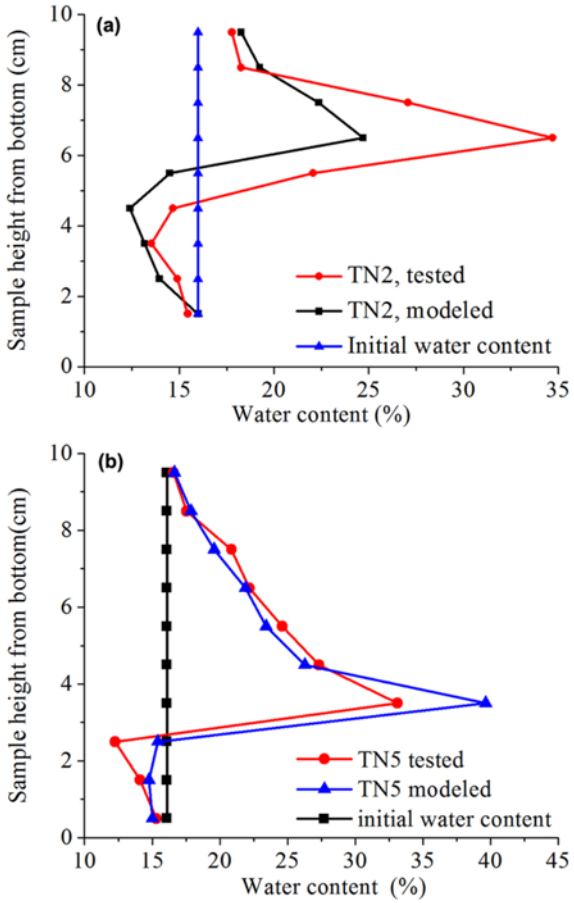

Fig. 16. Comparison of water content distribution. (a) In tests TN1 and TN2; (b) In tests TN2 and TN5.

position of the freezing fronts during modeling are 5.78 and 5.69 cm. These frozen depth curves have similar change laws and little difference in value. It can be concluded that the penetration of the freezing front is not sensitive to overburden pressure.

As is shown in Figure 14, the curves of water intake flux can be divided into two parts: increase and decrease parts. It can be seen that water intake does not occur immediately at the beginning of the test, and the water intake flux is constantly changing with elapsed time and has a peak value. This can be explained that water, which is drawn up to the growing ice lens, must go through the frozen fringe. As we know, the

permeability of the frozen fringe is very low, and becomes poor with increasing thickness (O'Neill and Miller, 1985). Equation (7) indicated that when the temperature is unchanged, the pore water pressure will also remain unchanged. Thus, according to Darcy's law, the water intake flux declines after it rises to a peak value.

The variation in frost heave is shown in Figure 15. Numerical simulation and laboratory experimental studies indicate there is no obvious frost heave occurs at the initial stage, before about 10 hours. After the frost heave occurs, the amount of frost heave increased with the elapsed time. It is obvious that an increase in the overburden pressure results in a reduction in the frost heave. From Figure 15, it can be seen that the modeled results are in good agreement with the test results.

Figure 16 shows the distribution of total water content versus the height of the soil sample. It can be seen that the calculated results agree with the tested results. Both the tested results and simulated results have a similar change law: (1) Water content becomes larger and larger and rises up to a peak value, then descends to the minimum, and finally increases gradually to the initial value. (2) The water contents are different in different areas: it increases in the frozen area and decreases in the unfrozen area, as shown in Figure 16. In Figure 16a, it can also be seen that water content in test TN5 is larger than that in test TN2. It could be concluded that the overburden pressure will decrease the amount of moisture migration.

7. DISCUSSION

Section 6 indicates that the presented model is suitable for describing the ice lens growth in freezing soil. Nevertheless, there are still some problems, such as disjoining pressure, deformable porous media, consolidation, and the relationship between ice lenses and water migration. These problems must be answered to give a complete picture of the physics of frost heave.

According to the experimental results, we deduce from unidirectional freezing tests that the initial segregation of ice in freezing soil is seemingly crack-like in nature. In order to elucidate the mechanisms in the ice lens segregation process, the authors assumed that the horizontal cracks mainly belong to stress cracks, and a new ice lens initial criteria was presented (Eq. 24). It can be seen that the stress criteria include two stresses: the dominant driving force for ice lens formation (the disjoining pressure P_{Lh}), and the constraining force (the sum of overburden pressure and tensile strength). The former is the mainly force that results in ice lens formation, and the latter is the force that blocks the ice lens formation. The previous studies indicated that driving force for ice lens formation can be pore ice pressure (O'Neil and Miller, 1985; Nixon, 1991; Akagawa et al., 2006), pore water pressure (Sheng et al., 1995; Zhou and Li, 2012), and ice-water pressure (Dash et al., 2006; Rempel, 2011). At a low temperature, the pore water will be quickly freezes, and the pore ice pressure quickly increases to the magnitude of the overburden pressure before ice nucleation (Thomas et al., 2009). It is well known that in soil types such as silty, clay, and loam, most of the water (pore water) will freeze at the freezing point but some liquid water still remains at sub-freezing temperatures. Therefore, elevation of the pore ice pressure could not be regarded as an ice lens initiation condition. Due to the curved interface, the ice pressure is different from the disjoining pressure P_{Lh} (Giplin, 1980). Thus, we considered the relative pressure of the liquid layer at the ice-water interface to be the primary force causing the soil to split and initiating ice lens formation. The disjoining pressure P_{Lh} is, in a sense, similar to the pore ice pressure, pore water pressure, and ice-water pressure. The difference is due to the stress-partitioning factor, which is influenced by the temperature and other factors.

The previous studies indicated that the ice-water interfacial tension (Giplin, 1980), the cohesive force (He et al., 2000), and overburden pressure (Akagawa et al., 2006) has been suggested as a part of the constraining force. In a conclusion, the constraining force should consider the effect of the physical properties of the soil medium, such as its microstructure, cohesive force and frictional force. However, it is hard to measure the interface curvature, the particle radius and the surface tension. The constraining force preventing soil cracking includes the external constraining force and internal constraining force and the internal constraining force can be cohesive force, tensile strength and other force. Tensile strength, as a macro physical and mechanical property, can reflect the effect of these factors on the separation strength. Thus, from the view of Giplin (1980), we considered the sum of overburden pressure and tensile strength as the separation strength, and when the disjoint pressure exceeded separation pressure, a new ice lens formed. Another problem, the tensile strength of the freezing soil requires the determinate of the segregation temperature. However, as we mentioned in the introduction, there is no specified method to measure the segregation temperature. Thus, we determined the ice lens initiation temperature from the monitored data. Based on the measured temperature profile and the location of the bottom of the growing ice lens, it is found that the temperature at the bottom of the last ice lens was closed to –0.2 °C. This is an approximate ice lens initiation temperature. Nevertheless, in this paper, the value of –0.2 °C was adopted. The indirect tensile test was conducted at this temperature, and the tensile strength of the soil $\sigma_t = 110$ kPa was determined. Furthermore, the tensile strength σ_t is influenced by many factors such as soil properties, water content, loading ratio, and so on. Thus, when σ_t was used as a part of separate strength, the value of σ_t should be noted.

From Figure 11, it can be seen that in the unfrozen zone, the pore water pressure is negative. According to the effective stress principle, the effective pressure increases gradually

with a decrease of pore water pressure. An increase in the effective stress leads to a decrease in the porosity (Fig. 10). As a result, the unfrozen soil is consolidated. However, the frost heave model, such as the rigid ice model (O'Neill and Miller, 1985; Zhou and Zhou, 2012) assumed that the freezing soil is incompressible, and include only heat and mass transport in the soil-freezing process. Thus, any consolidation that may occur due to pore water migration would not be taken into consideration. Peppin et al. (2008) also demonstrated that the interaction of the freezing front with the particles causes local consolidation. Thus, in this paper, the soil deformation was considered in the frost heave model. From Figure 10, it can be seen that the length of the black part, which lies under the ice lens, is decreasing with elapsed time. This can be explained that due to water migration and phase change, porosity decreases in the unfrozen zone, while the consolidation process is in progress in the freezing process. However, due to the different pore water pressure levels at different positions, the consolidation degree is different, which results in different change ratios of porosity at different positions (Fig. 10). In the frozen zone, water migrated from the unfrozen zone to the freezing front and stored behind the frozen fringe. This leads to a increase in the porosity, promotes the frost heave. Consequently, the deformation of freezing soil consists of the consolidation in the unfrozen zone and frost heave in the frozen zone.

8. CONCLUSIONS

This paper presents a theoretical framework of ice lens formation and growth in freezing porous media. The presented model, which is solved by way of a transient finite element approach, considers the following processes, including phase change, water transfer, soil deformation and the development of ice lenses. Numerical modeling of soil freezing and ice lens growth is presented, and verified by experimental results.

(1) The frost heave model is composed of two aspects: the coupled heat-mass transport and the growth of ice lens. A comprehensive stress criterion, which considered the effect of soil properties, is provided to determine the formation of a new ice lens, and the tensile strength was taken as the segregation strength. The formation of ice lenses becomes difficult with an increase of overburden pressure and tensile strength. The thickness of the ice lens is controlled by the water migration.

(2) A negative pore water pressure appears in the unfrozen zone under the frozen fringe, as a result of minus temperature. Due to water migration, the consolidation process and expansion process are in progress in the freezing process. Owing to different negative pore water pressure, different consolidation degrees occurred in the unfrozen soil. The deformation of freezing soil consists of the consolidation in the unfrozen zone and frost heave in the frozen zone.

(3) The temperature curve can be divided into the fast freezing section, the transitional section and the stable section. The water intake flux is constantly changing with elapsed time. Substantial water was stored in the frozen zone. Due to the limitation of water migration, ice lens formed different cryogenic structure in different sections, and this result in apparent oscillation exists in the distributions of water content.

ACKNOWLEDGMENTS: This work is supported by the National Natural Science Foundation of China (No. 41271080); the National Science and Technology Support Program (No. 2014BAG05B03) and the Funding of the State Key Laboratory Frozen Soil Engineering (No. SKLFSE-ZQ-35).

REFERENCES

Akagawa, S. and Nishisato, K., 2009, Tensile strength of frozen soil in the temperature range of the frozen fringe. Cold Regions Science and Technology, 57, 13–22.

Akagawa, S., Satoh, M., Kanie, S., and Mikami, T., 2006, Effects of tensile strength on ice lens initiation temperature. Proceedings of the 13th International Conference on cold region engineering, Orono, July 23–26, p. 1–12.

Azmatch, T.F., Sego, D.C., Arenson, L.U., and Biggar, K.W., 2011, Tensile strength and stress-strain behavior of Devon silt under frozen fringe conditions. Cold Regions Science and Technology, 68, 85–90.

Azmatch, T.F., Sego, D.C., Arenson, L.U., and Biggar, K.W., 2012, New ice lens initiation condition for frost heave in fine-grained soils. Cold Regions Science and Technology, 82, 8–13.

Bronfenbrener, L. and Bronfenbrener, R., 2010, Modeling frost heave in freezing soils. Cold Regions Science and Technology, 61, 43–64.

Cao, H.Z. and Liu, S., 2007, One dimension simulation of the rigid ice model of saturated freezing granular soil. Journal of Glaciology and Geocryology, 29, 32–38. (in Chinese with English abstract)

Dash, J., Rempel, A., and Wettlaufer, J., 2006, The physics of premelted ice and its geophysical consequences. Reviews of Modern Physics, 78, 695–741.

Derjaguin, B.V. and Churaev, N.V., 1978, The theory of frost heaving. Journal of Colloid and Interface Science, 67, 391–396.

Harlan, R.L., 1973, Analysis of coupled heat-fluid transport in partially frozen soil. Water Resources Research, 9, 1314–1323.

He, P., Cheng, G.D., and Yang, C.S., 2000, A couple model of heat, water and stress fields of saturated soil during freezing. Journal of Glaciology and Geocryology, 22, 135–138. (in Chinese with English abstract)

Gilpin, R.R., 1979, A model of the "liquid-like" layer between ice and a substrate with applications to wire regelation and particle migration. Journal of Colloid and Interface Science, 68, 235–251.

Gilpin, R.R., 1980, A model for the prediction of ice lensing and frost heave in soils. Water Resources Research, 16, 918–930.

Guymon, G.L. and Luthin, J.N., 1974, A coupled heat and moisture transport model for arctic soils. Water Resources Research, 10, 995–1001.

Konrad, J.M. and Morgenstern, N.R., 1980, A mechanistic theory of ice lens formation in fine-grained soils. Canadian Geotechnical Journal, 17, 473–486.

Konrad, J.M. and Morgenstern, N.R., 1981, The segregation potential of a freezing soil. Canadian Geotechnical Journal, 18, 482–491.

Konrad, J.M. and Duquennoi, C., 1993, A model for water transport

and ice lensing in freezing soils. Water Resources Research, 29, 3109–3124.
Mackay, J.R., 1974, Reticulate ice veins in permafrost, northern Canada. Canadian Geotechnical Journal, 11, 230–237.
Michalowski, R.L. and Zhu, M., 2006, Frost heave modelling using porosity rate function. International Journal for Numerical and Analytical Methods in Geomechanics, 30, 703–722.
Nicolsky, D.J., Romanovsky, V.E., and Panteleev, G. G., 2009, Estimation of soil thermal properties using in-situ temperature measurements in the active layer and permafrost. Cold Regions Science and Technology, 55, 120–129.
Nixon, J.F., 1991, Discrete ice lens theory for frost heave in soils. Canadian Geotechnical Journal, 28, 843–859.
O'Neill, K. and Miller, R.D., 1985, Exploration of a rigid ice model of frost heave. Water Resources Research, 21, 281–296.
Patterson, D.E. and Smith, M.W., 1981, Measurement of unfrozen water content by time domain reflectometry: Results from laboratory tests. Canadian Geotechnical Journal, 18, 131–144
Peppin, S., Wettlaufer, J., and Worster, M., 2008, Experimental verification of morphological instability in freezing aqueous colloidal suspensions. Physical review letters, 100, 238301.
Rempel, A.W., 2011, Microscopic and environmental controls on the spacing and thickness of segregated ice lenses. Quaternary Research, 75, 316–324.
Sheng, D., Axelsson, K., and Knutsson, S., 1995, Frost heave due to ice lens formation in freezing soils 1. Theory and verification. Nordic Hydrology, 26, 125–146.
Takagi, S., 1979, Segregation freezing as the cause of suction force for ice lens formation. Engineering Geology, 13, 93–100.
Taylor, G.S. and Luthin, J.N., 1978, A model for coupled heat and moisture transfer during soil freezing. Canadian Geotechnical Journal, 15, 548–555.
Thomas, H., Cleall, P., Li, Y.C., Harris, C., and Kern-Luetschg, M., 2009, Modelling of cryogenic processes in permafrost and seasonally frozen soils. Geotechnique, 59, 173–184.
Viklander, P., 1998, Permeability and volume changes in till due to cyclic freeze-thaw. Canadian Geotechnical Journal, 35, 471–477.
Xu, X.Z. and Deng, Y.S., 1991, Experimental study on water migration in freezing and frozen soils. Science Press, Beijing, 256 p.
Zhang, L.H., Ma, W., Yang, C.S., and Yuan, C., 2014, Investigation of the pore water pressures of coarse grained sandy soil during open-system step-freezing and thawing tests. Engineering Geology, 181, 233–248.
Zhou, J.Z. and Li, D.Q., 2012, Numerical analysis of coupled water, heat and stress in saturated freezing soil. Cold Regions Science and Technology, 72, 43–49.
Zhou, J.Z., Wei, C.F., Wei, H.Z., and Tan, L., 2014, Experimental and theoretical characterization of frost heave and ice lenses. Cold Regions Science and Technology, 104–105, 76–87.
Zhou, Y. and Zhou, G.Q., 2012, Intermittent freezing mode to reduce frost heave in freezing soils – experiments and mechanism analysis. Canadian Geotechnical Journal, 49, 686–693.

Manuscript received July 27, 2015
Manuscript accepted January 24, 2016